crystals

MDPI

Article

Effect of Precipitated Precursor on the Catalytic Performance of Mesoporous Carbon Supported CuO-ZnO Catalysts

Yandong Li [1,2,*], Guangfen Liang [2], Chengrui Wang [2], Yanhong Fang [2] and Huamei Duan [2,*]

[1] Chongqing Key Laboratory of Extraordinary Bond Engineering and Advanced Materials Technology, Yangtze Normal University, Chongqing 408100, China
[2] Laboratory of Metallurgy and Materials, College of Materials Science and Engineering, Chongqing University, Chongqing 400044, China; liangguangfen@cqu.edu.cn (G.L.); wangchengrui@cqu.edu.cn (C.W.); fangyanhong@cqu.edu.cn (Y.F.)
* Correspondence: liyd@yznu.edu.cn (Y.L.); duanhuamei@cqu.edu.cn (H.D.)

Abstract: As part of concepts for chemical energy storage of excess chemical energy produced from renewable sources, we investigated the performance of CuO/ZnO catalysts supported on mesoporous carbon to convert CO_2 hydrogenation to methanol. In this work, mesoporous carbon was used as the catalyst support for CuO-ZnO catalysts. Four catalysts with different precipitated precursors were synthesized and analyzed by N_2-physisorption, X-ray diffraction (XRD), thermogravimetric analysis (TG-DTG), scanning electron microscopy (SEM) and transmission electron microscopy (TEM). The results show that catalyst CZ-in situ had the highest turnover frequency (TOF) (2.8×10^{-3} s^{-1}) and methanol production rate (0.8 mmol $g^{-1} \cdot h^{-1}$). The catalysts for co-precipitation of copper and zinc on carbon precursors are more active. Cu/ZnO domains that are accessible to the reactant gas are another reason for the catalysts being active. The Cu-ZnO interface is crucial to methanol catalyst activity.

Keywords: mesoporous carbon; CO_2 hydrogenation to methanol; precipitated precursor; catalytic performance

Citation: Li, Y.; Liang, G.; Wang, C.; Fang, Y.; Duan, H. Effect of Precipitated Precursor on the Catalytic Performance of Mesoporous Carbon Supported CuO-ZnO Catalysts. *Crystals* **2021**, *11*, 582. https://doi.org/10.3390/cryst11060582

Academic Editors: Fatih Gulec, Yongliang (Harry) Yan, Peter Clough and Vladislav V. Kharton

Received: 10 April 2021
Accepted: 11 May 2021
Published: 22 May 2021

1. Introduction

Rapid economic development cannot be separated from firm dependence on fossil fuel. However, the cost is rising CO_2 emissions. Because of the consumption of fossil fuel, the original balance between carbon and oxygen is broken, which leads to a series of serious problems, such as global warming, sea level rise and Arctic glacier melting [1–3]. According to the statistics of the International Energy Agency (IEA), global energy-related carbon dioxide (CO_2) emissions plateaued in 2019 at 33.3 Gt. Compared with 2010 (30.4 Gt), they increased by 9.54% [4]. Therefore, how to reduce CO_2 emissions and convert carbon dioxide into other chemical raw materials have aroused the interest of researchers [5,6]. Among these techniques, CO_2 hydrogenation to methanol is one of the most effective and economical ways to reduce CO_2 emission [7,8]. In this way, the closed-loop utilization from fossil fuel to CO_2 and then from CO_2 to fuel can be realized.

CO_2 has stable chemical properties and the dissociation energy of the C=O bond reaches up to 750 kJ·mol^{-1} [9]. Therefore, catalysts have been becoming the core of methanol industrial synthesis processes. At present, Cu/ZnO-based [10,11] catalysts have been widely applied and prepared by the co-precipitation method [12,13]. Obviously, the catalytic performance is significantly influenced by different preparation conditions and features of the catalyst materials. Two key factors are the phase and composition of the catalyst precursor. The effect of the precursor on methanol catalyst activity has been reported in many studies [14–17]. Himelfarb et al. [18] studied the co-precipitation method with a Cu/Zn ratio of 3:7, resulting in only a $(Cu_{0.3}Zn_{0.7})_5(CO_3)_2(OH)_6$ phase in the precursor. Pollard [19,20] studied the phase transition process of the precipitates in the

mother liquor. Firstly, the reaction generated amorphous basic cupric carbonate georgeite ($Cu_2CO_3(OH)_2$). Then, it transformed into crystalline malachite ($Cu_2CO_3(OH)_2$) gradually during the aging process. Finally, zincian malachite (Cu, Zn)$_2CO_3(OH)_2$ could be formed and it was the only precursor for the formation of highly active catalysts. Li [19] claimed that georgeite was also a possible candidate for the catalyst precursor. While azurite as a precursor for preparing a methanol synthesis catalyst is active, the performance is inferior to zincian malachite. There is controversy regarding catalyst precursors. In this paper, we report the different Cu or Zn precursors for the catalysts. The role of catalyst precursors may be more complex than that had been realized before.

High surface-area supports generally contain mesopores and micropores that are important to the activity and selectivity. Mesoporosity is preferred over microporosity for most catalytic applications because a mesoporous network can make reactants and products more convenient for diffusion [21]. Van Den Berg and coworkers [22,23] were the first researchers to report the function of mesoporous silica as the support for methanol synthesis catalysts and it showed many advantages. Mesoporous carbon has a similar structure to mesoporous silica. However, different surface chemistry has not been investigated in methanol synthesis. In 2014, our findings [24] suggested that these FDU-15 carbon-supported Cu and ZnO catalysts showed advantages for CO_2 conversion and may potentially be better catalysts for methanol production. In the same year, we proposed a facile method for synthesis of a mesoporous carbon-supported methanol catalyst containing well dispersed Cu/ZnO. The results proved that this was an effective way to control the dispersion of metal oxide particles [25]. In 2017, we investigated the catalytic performance of a Cu/ZnO catalyst supported on mesoporous carbon FDU-15, which was closely related to the factors of calcination temperature, ramping rate and metal loading [26]. Those results confirmed that mesoporous carbon was a very promising catalyst support for methanol conversion.

In order to address the effect of the Cu/Zn precursors on the catalytic performance, we investigated four catalysts with different catalyst precursors supported by mesoporous carbon FDU-15 (MC). The precursors and the catalysts were characterized by the means of N_2-physisorption, XRD, TG-DTG, SEM and TEM. The catalytic performances were tested in a fixed-bed reactor.

2. Experimental

2.1. Materials

$Cu(NO_3)_2{\cdot}2.5H_2O$; $Zn(NO_3)_2{\cdot}6H_2O$, Pluronic F127, formaldehyde solution (37 wt.%), phenol, sodium carbonate, sodium hydroxide and anhydrous ethanol were analytical regents and were purchased from Sigma–Aldrich Chemicals Corp. New South Wales, Australia. All the reagents were purchased and used without further purification.

2.2. Experimental Method

2.2.1. Preparation of Stage A Phenolic Resin Pre-Polymers

Stage A phenolic resin is a kind of soluble phenolic resin with a low molecular weight, which was prepared from phenol and formaldehyde under the condition of alkali catalysis [27]. Firstly, 9.15 g phenol was dissolved in deionized water at 40–42 °C. Then, the 20 wt.% NaOH solution (1.95 g) was added and stirred for 10 min. Next, 37 wt.% formaldehyde solution (15.75 g) was added, and then the temperature was raised to 70–75 °C for 1 h. Finally, the temperature was cooled to room temperature, and the pH adjusted to pH = 7–8 with 0.6 mol/L HCl solution. The mixture was dehydrated to a viscous liquid (1–2 h) under vacuum at less than 50 °C. The viscous liquid was dissolved in ethanol to form a uniform solution with a concentration of 20 wt.% for standby.

2.2.2. Synthesis of Mesoporous Carbon (MC)

MC was prepared by a solvent volatilization-induced self-assembly process in ethanol solution by using phenolic resin as the polymer precursor and F127 as the template. In this

process, the ratio of phenolic resin: F127: ethanol was 1:1:20 (mass ratio). Generally, we dissolved F127 (4.0 g) in ethanol (20 g) and stirred the solution until clarification. Then, we added 20 g 20 wt.% of the stage A phenolic resin ethanol solution into the solution. After that, we added the required ethanol solution to meet the set proportion of the solution, and stirred for 30 min to obtain a uniform solution. The solution was transferred to the dish, kept at room temperature for 5 h, and then the dish was kept in a 100 °C oven for 24 h to obtain transparent film materials. The material was scraped off the dish and ground to powder, and as-made FDU-15 was recorded. MC was obtained by roasting as-made FDU-15 in a tube furnace under N_2 protection. The roasting conditions were as follows: N_2 flow rate was 50 $cm^3 \cdot min^{-1}$, heating rate was 2 °C·min^{-1}, constant temperature was kept at 350 °C for 2 h, then temperature was increased to 700 °C for 2 h at the same heating rate, and then reduced to room temperature in an N_2 atmosphere.

2.2.3. MC Supported Catalyst Prepared by Precipitation Method

The catalysts were prepared by the precipitation method. A certain amount of nitrate was dissolved in a flask with 50 mL deionized water. The flask was placed in a magnetic stirring oil bath with a stirring speed of 300 r·min^{-1} at a temperature between 68 and 72 °C. We added 8 wt.% sodium carbonate solution to adjust to pH = 7–8 under continuous stirring. We maintained the pH and aging for 3 h. This was followed by filtration and the separated solids were rinsed several times with deionized water. The solid was dried at 100 °C for 10 h. The precipitated precursor of Cu was denoted as Cu precipitate. The precipitated precursor of zinc was denoted as Zn precipitate, and the precursor of Cu and Zn was denoted as Cu Zn precipitate. The Cu Zn precipitate was added to the homogeneous solution stage A phenolic resin and ethanol of F127. The rest conditions were the same with MC and the carbonization temperature was 700 °C. The catalyst was denoted as CZ-post-precipitation (CZ-post). Cu precipitate was added to the stage A phenolic resin, F127 and zinc nitrate in ethanol solution. The rest of the conditions were the same with CZ-post. This catalyst was denoted as C-post-precipitation (C-post). Zn precipitate was added to the homogeneous stage A phenolic resin, F127 and zinc nitrate in ethanol solution and the rest of the conditions were the same as for preparation of C-post. This catalyst was denoted as Z-post. A certain amount of MC was placed in a flask containing 50 mL deionized water, to which was added the required copper nitrate and zinc nitrate. The 8 wt.% sodium carbonate solution was added to adjust to pH = 7–8. The remaining steps were the same as for the preparation method of the precipitated precursor. The product was roasted in an N_2 atmosphere at 300 °C for 3 h, and the catalyst was denoted as CZ-in situ.

2.3. Catalyst Characterization and Performance Testing

Nitrogen (N_2) physisorption analysis was measured on a Micromeritics TriStar sorption analyzer (Norcross, GA, USA) and a Micromeritics ASAP 2020 gas adsorption analyzer (Norcross, GA, USA) at −196 °C. Powder X-ray diffraction (XRD) analysis was performed on a Philips PW1130 powder diffractometer (Eindhoven, Dutch) with Cu Kα radiation (λ = 1.5405 Å) at 40 kV and 25 mA. Thermal decomposition was performed on an apparatus that enabled the simultaneous recording of TG and DTG signals (TGA/SDTA 851) in the temperature range 30–700 °C with a ramping rate of 2 °C/min under a nitrogen atmosphere. The metal loading of the four catalysts was obtained by burning off the carbon support in an O_2 atmosphere with a ramping rate of 2 °C/min. The morphology of the catalysts was investigated on a JEOL 7001F FEG scanning electron microscope (SEM) (Tokyo, Japan). The structural features of four catalysts were investigated by transmission electron microscopy (TEM) on a Philips CM20 (Eindhoven, Dutch) and FEI Tecnai F20 (Hillsboro, OR, USA).

Measurements of methanol synthesis activity were conducted in a fixed-bed stainless steel reactor. More details were included in our previous work [24]. One gram of catalyst was reduced in flowing dilute hydrogen (5% H_2 in Ar) at 543 K for 2 h. Then, methanol synthesis activity was measured at 40 bar and 260 °C with the GHSV = 3600 h^{-1}. The reactant

gas was composed of 25% CO_2 and 75% H_2. Concentrations of the product were analyzed using an online refinery gas analyzer (Clarus 580 GC; PerkinElmer, Waltham, MA, USA). Water was removed by cooling the product gas to −1 °C. Then, analyses were conducted under isothermal conditions at 22 °C. Product gas compositions were determined with reference to a series of calibration curves, which were constructed from the analysis of five standard gas mixtures.

3. Results and Discussion

3.1. N_2 Physisorption

The N_2 physisorption results for four catalysts are shown in Figure 1. The catalyst of CZ-post presented a typical IV-type adsorption curve and H2 hysteresis loop. The adsorption curves of C-post and Z-post were type II and type I, respectively, and the hysteresis loops were type H4 and type H3 (without closure) [28]. These results indicated that both C-post and Z-post contained slit grooves formed by gathered particles (disclike or small cubes). The pore shape and size of C-post was more inerratic, while Z-post was irregular. CZ-in situ presented a typical IV-type adsorption curve and H1-type hysteresis loop, and the predominant adsorption finished between P/P0 = 0.6 and 0.7, which was a characteristic of the mesopores in the material. The results show that the samples loaded with Cu and Zn still had regular mesoporous channels.

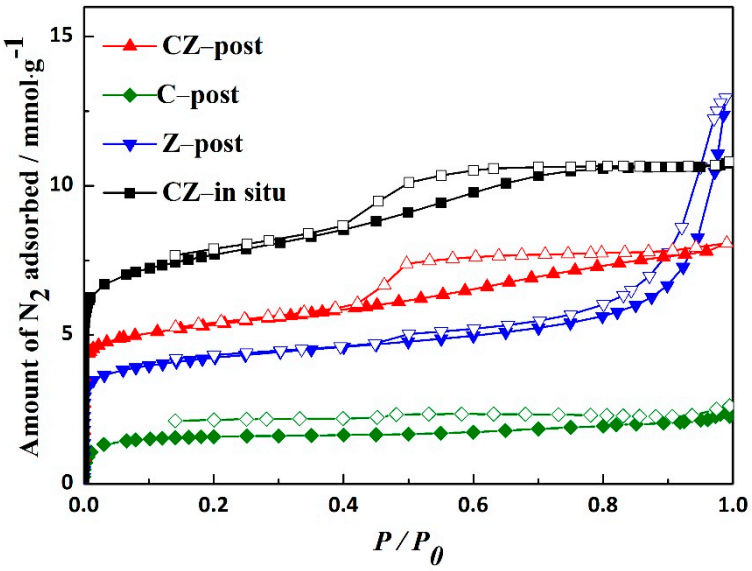

Figure 1. N_2 adsorption and desorption isotherms of catalysts under 196 °C.

The pore size distribution of catalysts prepared by the precipitation method are shown in Figure 2. Micropores and mesoporous structures were discovered in the catalyst CZ-post. The highest frequency of micropores was 0.6 nm. The mesoporous distribution range was from 2 to 9 nm, and the highest occurrence frequency was 5 nm. From the pore size distribution curves, it can be seen that the micropores of C-post and Z-post were gathered in the range of 1–2 nm, and there were almost no mesoporous pores. The highest microporous frequency of catalyst CZ-in situ appeared at 0.6 nm, the mesoporous distribution was from 2 to 8 nm, and the highest frequency was 6 nm.

It can be concluded that the distribution of pore size was significantly affected by the calcination temperature and precursors, and a higher roasting temperature in a certain range and carbonization before adding the precursor would benefit pore structure development.

Table 1 summarizes the results for BET surface area, specific pore volume, micropore volume and mesoporous pore volume of the four catalysts. The BET surface area and pore volume of CZ-post were 416 $m^2 \cdot g^{-1}$ and 0.28 $cm^3 \cdot g^{-1}$, respectively. The pore volumes of micropores and mesopores were 0.18 and 0.09 $cm^3 \cdot g^{-1}$, respectively. The BET surface area

of C-post was 166 $m^2 \cdot g^{-1}$. The pore volume was 0.11 $cm^3 \cdot g^{-1}$. The micropore volume and mesoporous pore volume were 0.05 and 0.06 $cm^3 \cdot g^{-1}$. The specific surface area of Z-post was 329 $m^2 \cdot g^{-1}$, the pore volume was 0.45 $cm^3 \cdot g^{-1}$ and the microporous volume was 0.09 $cm^3 \cdot g^{-1}$. For catalysts C-post and Z-post, the total pore volume without micropore volume was the sum of the mesoporous and large-pore volume. The mesoporous volume could not be found in the PSD curve. Therefore, the large-pore volumes of two catalysts were 0.06 and 0.36 $cm^3 \cdot g^{-1}$, respectively. The BET surface area of CZ-in situ was 596 $m^2 \cdot g^{-1}$. The pore volume was 0.37 $cm^3 \cdot g^{-1}$. The pore volume and mesoporous pore volume were 0.26 and 0.11 $m^3 \cdot g^{-1}$, respectively.

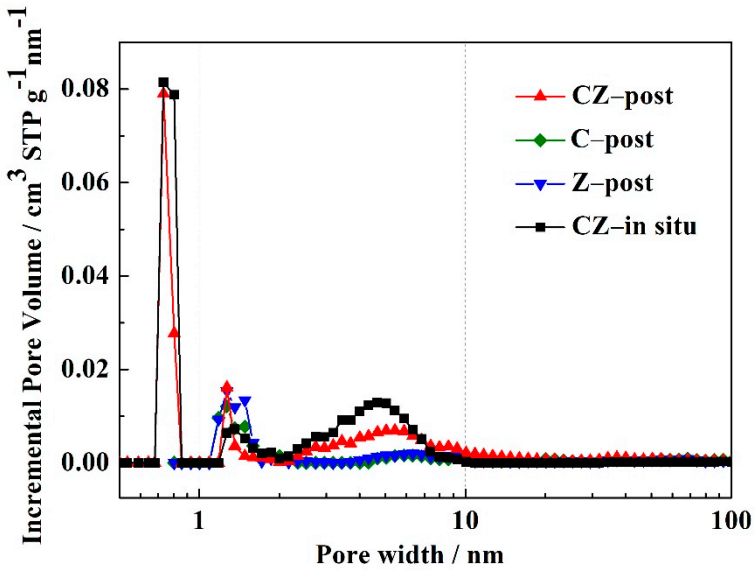

Figure 2. Pore size distribution curves of catalysts.

Table 1. Surface area and pore volumes of catalysts.

Catalyst Name	BET Surface Area ($m^2 \cdot g^{-1}$)	Pore Volume ($cm^3 \cdot g^{-1}$)	Vmicro ($cm^3 \cdot g^{-1}$)	Vmeso + Vmacro ($cm^3 \cdot g^{-1}$)
CZ-post	416	0.28	0.18	0.09
C-post	166	0.11	0.05	0.06
Z-post	329	0.45	0.09	0.36
CZ-in situ	596	0.37	0.26	0.11

It can be concluded that the surface area and pore volume were significantly affected by the precipitated precursor. The precipitated precursors of Cu and Zn were deposited on the carbon surface or carbon channel structure directly, which resulted in CZ-in situ with the highest BET surface. When the precursor of Cu Zn precipitate was added and there was co-precipitation of Cu and Zn on the MC support, a higher BET surface area and regular channel structure could be generated in the catalyst. The BET specific surface area of the catalyst generated by adding only one of the precipitated precursors was small, and no mesoporous formation occurred.

3.2. X-ray Diffraction

Figure 3a shows the XRD patterns of different precipitated precursors. The XRD pattern of the Zn precipitate shows that the crystal of the precipitated precursor was Zn_4CO_3 $(OH)_6 \cdot H_2O$ (PDF No.11-287) and the crystal size was about 11 nm determined by Scherrer's equation. The XRD pattern of the Cu precipitate shows that the precursor was a mixture of Cu_2 $(OH)_3$ NO_3 (PDF No. 15-14) and CuO (PDF No. 80-76). The crystal size of $Cu_2(OH)_3NO_3$ was 68 nm. The strength of CuO was too small to be calculated by Scherer's

formula [29]. The XRD pattern of the Cu Zn precipitate showed that the precursor was amorphous with a very broad peak packet (2θ = 30–40°). Li [19] studied the influence of pH value and reaction temperature on the catalyst precursor. The results showed that it was conducive to generate $Cu_2(OH)_3NO_3$ when the pH value was less than 6. The PH of the precipitate prepared in this manuscript is more than 7, while it still generated $Cu_2(OH)_3NO_3$. This is different to the literature.

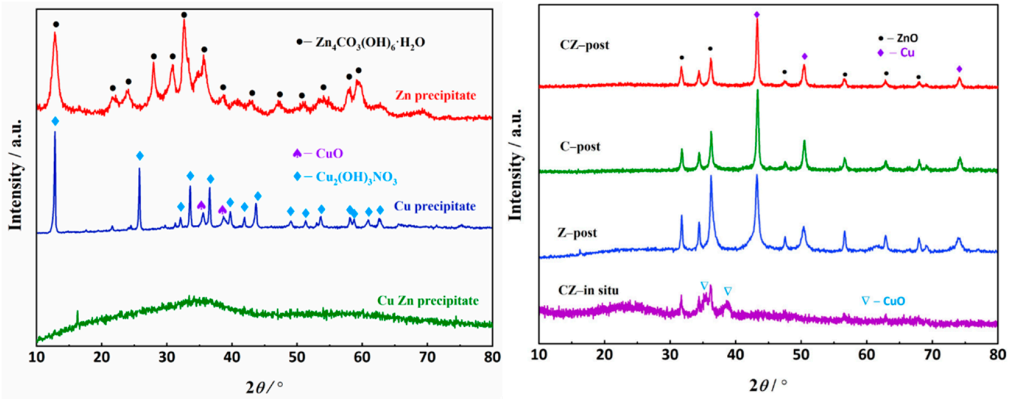

Figure 3. XRD spectra of (**a**) precipitated precursors; (**b**) four catalysts.

The XRD pattern of catalysts is shown in Figure 3b. It can be seen that the sharp diffraction peaks of Cu (PDF No.04-0836) and ZnO (PDF No. 89-0510) both appeared in the catalysts of CZ-post, C-post and Z-post. Those results show that both Cu and ZnO components in these catalysts were well crystallized. The Cu and ZnO crystal sizes of CZ-1 were about 14 nm. For C-post, the Cu and ZnO crystal sizes were 18 nm and 20 nm, respectively. For Z-post, they were about 27 nm. For CZ-in situ, the XRD spectra had sharp ZnO peaks, and the crystal size of ZnO was about 11 nm. The CuO spectra were very broad and had low intensity. The broadness of peak suggests that the crystal size of CuO (PDF No. 80-76) was very small.

From these results, it can be seen that the precipitated precursors of single precipitation were all well crystallized (CZ-post, C-post, and Z-post), and the co-precipitation products were amorphous (CZ-in situ). Cu and ZnO crystals appeared in the catalysts CZ-post, C-post, and Z-post. ZnO and CuO were observed in the catalyst CZ-in situ. Besides, CuO was not reduced to Cu during roasting, and the crystal size of CuO was very small.

3.3. TG-DTG Analysis

The TG-DTG curves of different precipitated precursors and as-made FDU-15 with Cu Zn precipitate are shown in Figure 4a–d. According to Figure 4a, the total weight loss of the catalyst was 30%, which could be divided into two parts. The first part was below 300 °C with slow weight loss, which might be the loss of interlamellar water and surface water of the catalyst. Another part appeared between 400 and 500 °C, according to the analysis in the literature [30], which was the decomposition or release of CO_2 and water. According to the TG-DTG result of Cu precipitation (Figure 4b), the total weight loss of precipitated precursor was 28%, and it occurred from 150 to 250 °C. Combined with the results of XRD (Figure 3a), the weight loss was a result of the decomposition and release of H_2O and nitrides. For Zn precipitate (Figure 4c), its total weight loss was 34% with two stages. One stage appeared below 200 °C, which might be caused by the loss of interlamellar water and OH^- in $Zn_4CO_3(OH)_6 \cdot H_2O$ crystal [31]. The second stage appeared between 200 °C and 250 °C, which came from the further decomposition of OH^- and nitrous compounds. For as-made FDU-15 with Cu Zn precipitate (Figure 4d), the total weight loss was 60% in two stages. Combined with the weight loss of as-made FDU 15 and precipitated precursors, in the first stage, the weight loss was due to the water loss of the precipitated precursor.

The total weight loss was 10–15% within the range 230–250 °C. Another weight loss was about 50% within the range 250–400 °C. This was the common result of template F127 decomposition [27] and further decomposition of the precipitated precursor. It should be noted that the decomposition of as-made FDU-15 with Cu Zn precipitate was not a simple addition of Cu Zn precipitate and as-made FDU-15. Weightlessness appeared at a new location, which indicates that the mixing of these materials could decrease the decomposition temperature. The TG-DTG results were used to determine the calcination temperature of the catalysts. In order to ensure the full development of the pore structure of CZ-post, C-post and Z-post, the calcination temperature of these three catalysts was 700 °C. Since CZ-in situ was supported on MC, MC was obtained by calcining as-made FDU 15 at 700 °C. It should be noted that the full decomposition of the bulk Cu Zn precipitate was at about 454 °C. When supported on MC, the decomposition of the precursor could be reduced by forming small domains. Therefore, CZ-in situ was calcined at 300 °C only for the decomposition of Cu Zn precipitate.

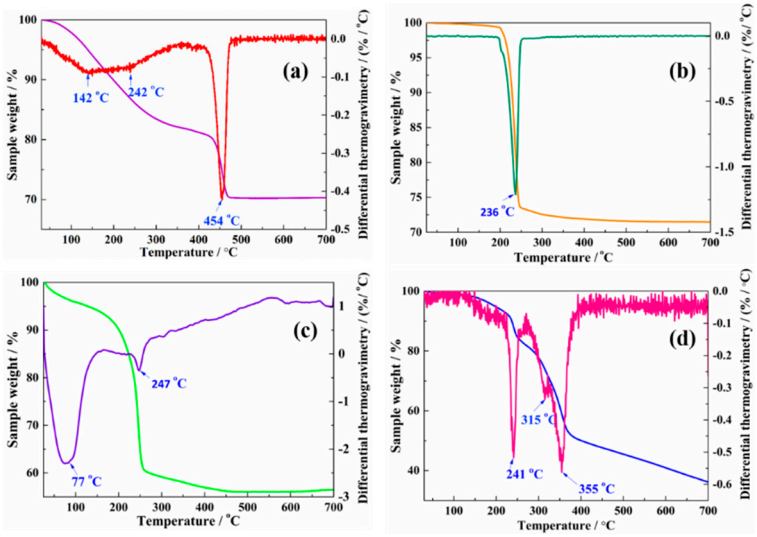

Figure 4. TG−DTG curves of precipitated precursors and as-made FDU-15 with Cu Zn precipitate. (**a**) Cu Zn precipitate; (**b**) Cu precipitate; (**c**) Zn precipitate; (**d**) as-made FDU-15 with Cu Zn precipitate.

3.4. SEM and EDX

3.4.1. SEM

Figure 5a–d show the SEM images of the catalysts. For CZ-post (Figure 5a), metals and metal oxides were wrapped in carbon support and dispersed evenly. For C-post (Figure 5b) and Z-post (Figure 5c), metal and metal oxides gathered on the surface of the support with a uniform particle size. Compared with four preparation methods of catalysts, it was easy to understand their distribution. For CZ-post, the precipitated precursor was dispersed in a FDU precursor solution to form membrane and carbonization. The precipitated precursor was wrapped by the carbon precursor during the membrane-making process. Therefore, the metal oxide after carbonization was also wrapped by the carbon support. For C-post and Z-post, they were different from crystal CZ-post. Both of them were added a precipitated precursor, while another precursor was dissolved in the carbon precursor. Therefore, some of the metals or metal oxides were deposited on the surface of the carbon support. In order to further understand the influence of precipitated precursor and nitrate precursor on the distribution of metal and metal oxides in the support, C-post and Z-post were performed by high-resolution SEM with EDX analysis, and the results and analysis are shown in Section 3.4.2. According to the XRD results (Figure 3), Cu and ZnO appeared in CZ-post, C-post and Z-post. Combined with the SEM results, Cu and ZnO in these catalysts had completely different distributions. For CZ-post, Cu and Zn nitrates were

co-precipitated after addition of Na_2CO_3 and then added to the carbon precursor solution. The precipitation contained the mixed Cu and Zn hydroxides that decomposed into mixed CuO and ZnO, which further reduced into Cu/ZnO during the carbonization step [24]. Since these metals and metal oxides were formed during the carbonization step, they were hidden in the carbon matrix and had a limited area accessible to the reaction gas. However, because a precipitate was formed in the first step, this ensured the formation of Cu and ZnO in close proximity. For CZ-in situ, Cu Zn precipitate was formed after the carbon formation, and it was distributed on the surface of the carbon supports.

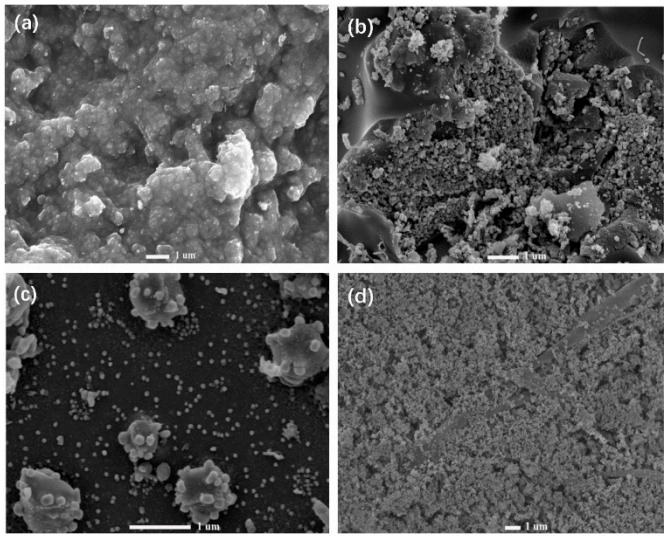

Figure 5. SEM images of catalysts: (**a**) CZ-post; (**b**) C-post; (**c**) Z-post; (**d**) CZ-in situ.

Combined with the XRD results, CuO appeared in CZ-in situ instead of Cu. This might be due to the surface contact between the precipitated precursor and carbon support not being as strong as the other catalysts, and the carbon support could not reduce CuO. Maybe the carbon support could not reduce the CuO to Cu at the calcination temperature of 300 °C.

3.4.2. EDX Analysis

Figure 6a–d show the EDX mapping of C-post. Figure 6b shows the element mapping of Cu; there was less Cu on the catalyst surface, which was due to the Cu precipitate in the preparation process of the catalyst being wrapped by the carbon precursor. After calcination, only some Cu metal particles were exposed on the surface. According to the O and Zn element mapping (Figure 6c,d), this was due to the ZnO particles on the surface of C-post. Figure 7a–d show that the metal or metal oxide particles of Z-post catalyst were Cu and ZnO. O elements almost occupied the entire surface of the catalyst, which could reveal that O had a corresponding high-brightness state where Zn appears, and when Cu appeared, the same high-brightness disappeared. Therefore, they were Cu^0 and zinc oxide, which was consistent with the XRD results. In addition to the O element from ZnO, the O element occupied the whole the carbon support. EDX spectra of the corresponding region of the catalyst C-post showed that Cu content was 4.1% and ZnO content was 55.6%. While Z-post was different from the catalyst C-post, the addition of Zn precipitation did not cause ZnO to be wrapped completely by the carbon support. A large amount of ZnO could be observed on the surface of the carbon support. According to the EDX results, the content of Cu was 52.7% and the Zn was 24.5%, which was close to the theoretical molar ratio of Cu:ZnO = 2:1. Therefore, it could be that the addition of Zn precipitate and $Cu(NO_3)_2 \cdot H_2O$ were conducive to the formation of evenly dispersed Cu and ZnO.

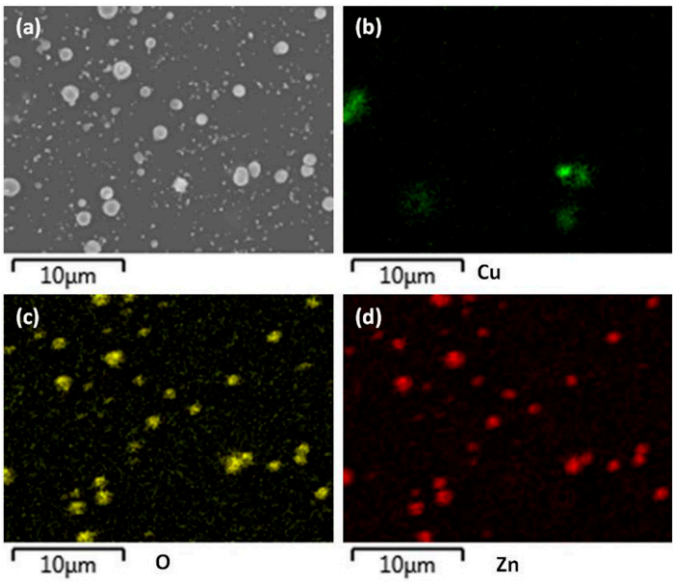

Figure 6. EDX mapping of catalyst C-post. (**a**) SEM image; (**b**) Cu element mapping; (**c**) O element mapping; (**d**) Zn element mapping.

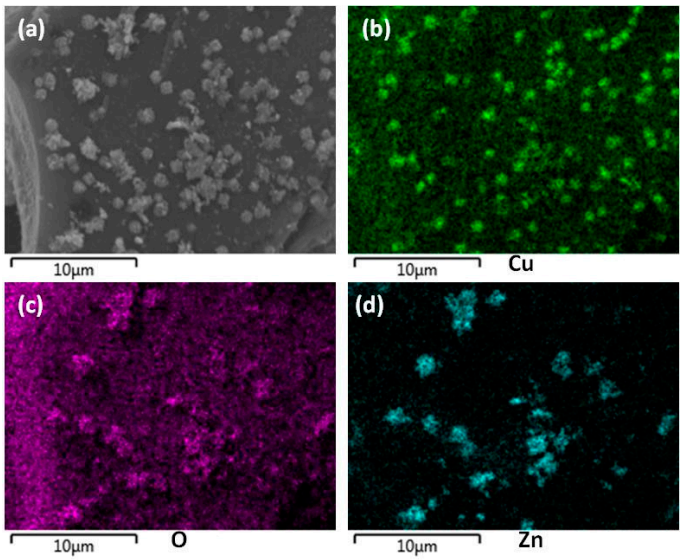

Figure 7. EDX mapping of catalyst Z-post. (**a**) SEM image; (**b**) Cu element mapping; (**c**) O element mapping; (**d**) Zn element mapping.

3.5. TEM Analysis

Figure 8a–d show the TEM images of the four catalysts. Most of the metal or metal oxide loaded on the CZ-post dispersed evenly. In addition, some of them were aggregated (Figure 8a). The size of the metal oxides was 30–70 nm. From the TEM results (Figure 8b,c), the metal and metal oxide distribution of C-post and Z-post were similar. For C-post, the loaded metal was dispersed on the carbon support with uniform particle sizes of 20–40 nm. Figure 8c shows that the nanoparticles of Z-post were distributed uniformly on the carbon matrix in the range 20–55 nm. The average size was about 41 nm. For catalyst CZ-in situ (Figure 8d), more than half of the particle sizes were 30–50 nm, which were Cu and Zn clusters composed of metal oxide particles.

From these results, it can be seen that the distribution of metal and metal oxides in the catalysts obtained by different precipitated precursors was different, whether they were embodied by carbon support or not.

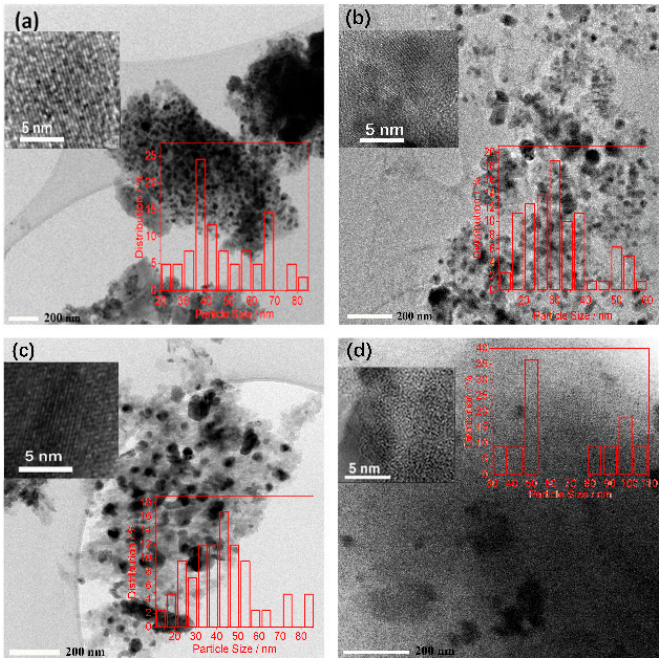

Figure 8. TEM images of catalysts. (**a**) CZ-post; (**b**) C-post; (**c**) Z-post; (**d**) CZ-in situ.

3.6. Catalytic Performance Test

3.6.1. Calculation of Methanol Formation Rate

Methanol formation rate is the mass–time yield per gram of catalyst, and the calculation method is shown in Equation (1).

$$CH_3OH\ formation\ rate\ (\mathrm{mmol \cdot g^{-1} \cdot h^{-1}}) = \frac{(CO_2\ conversion \times CH_3OH\ selectivity) \times n^{\mathrm{in}}_{CO_2}}{22.4 \times 10^3 \times m} \quad (1)$$

where m is the mass of the catalysts (g).

3.6.2. Calculation of Cu Surface Area

Cu surface area was measured by N_2O chemisorption on a Micromeritics Autochem HP 2950 apparatus [32,33]. The main equation involved is shown in Equation (2) [34]. Typically, 0.05 g catalyst was placed in a u-shaped tube. It was dried for 2 h at 120 °C under a He atmosphere, then heated up to 220 °C. It was reduced from Cu^{2+} to Cu^0 at 270 °C for 2 h under a H_2 atmosphere, and the temperature was reduced to 90 °C under a He atmosphere. Then, N_2O was introduced to oxidize Cu^0 to Cu^+. Meanwhile, N_2O was reduced to N_2 [35]. TCD detected the N_2 signal by comparing with the standard curve to determine the Cu surface area, and finally calculated the surface area of Cu by Equation (3).

$$2Cu + N_2O = Cu - O - Cu + N_2 \quad (2)$$

$$Cu\ surface\ area\ (\mathrm{m^2 \cdot g^{-1}}) = \frac{n \times SF \times \mathrm{N} \times s}{m} \quad (3)$$

where n is the mole number of N_2 formed in the reaction;
SF is the stoichiometric coefficient, 2;
N is Avogadro's constant, 6.02×10^{23};
s is each Cu atom area, 0.068×10^{-18} (m^2);
m is the mass of the catalyst (g).

3.6.3. Turnover Frequency (TOF)

The turnover frequency (TOF) of per unit Cu area was used to compare the intrinsic catalytic activity of different catalysts, and the calculation method is shown in Equation (4).

$$TOF(s^{-1}) = \frac{CH_3OH\ formation\ rate \times N \times s}{Cu\ surface\ area \times 3600} \quad (4)$$

where N is Avogadro's constant, 6.02×10^{23};
s is each Cu atom area (m^2);
Cu surface area is Equation (3).

3.7. Analysis of Catalytic Performance

The metal loading amount, effective Cu surface area, CO_2 conversion, methanol formation rate and TOF for catalysts are summarized in Table 2. The effective Cu surface areas of the four catalysts were in the range 0.5 to 3.3 $m^2 \cdot g^{-1}$, which was 2.9 $m^2 \cdot g^{-1}$ for CZ-post, 1.5 $m^2 \cdot g^{-1}$ for C-post, 0.5 $m^2 \cdot g^{-1}$ for Z-post and 3.3 $m^2 \cdot g^{-1}$ for CZ-in situ. The metal loading amounts of CZ-post, C-post, Z-post and CZ-in situ were 15, 35, 41 and 10%, respectively. CO_2 conversions of these four catalysts were 5.3, 3.5, 2.5 and 7.3%, respectively. It was known that high metal loading on the catalyst was important for high methanol conversion. The metal loading amounts of C-post and Z-post were far higher than the other catalysts, but both of them had little activity. Methanol formation rate results indicate that the catalyst of CZ-in situ produced a methanol rate of 0.8 $mmol \cdot g^{-1} \cdot h^{-1}$. It is worth noting that the TOF of CZ-in situ was 2.8×10^{-3} s^{-1} with the metal loading amount of 10%. Because of the precursors, the catalytic performances were different. The catalyst state may be more complex than has been realized before.

Table 2. Metal loading amount, effective Cu surface area, methanol formation rate and TOF of the catalysts.

Catalyst Name	Metal Loading Amount [a] (wt.%)	Cu-A [b] ($m^2 \cdot g^{-1}$)	CO_2 Conversion (%)	MTY [c] ($mmol \cdot g^{-1} \cdot h^{-1}$)	TOF [d] $\times 10^3$ (s^{-1})
CZ-post	15	2.9	5.3	0.4	1.5
C-post	35	1.5	3.5	0.05	0.4
Z-post	41	0.5	2.5	0.04	0.9
CZ-in situ	10	3.3	7.3	0.8	2.8

[a] Obtained from TGA tests in O_2 atmosphere. [b] Effective Cu surface area. [c] Mass–time yield per gram of catalyst. [d] TOF was calculated from the methanol formation rate and the number of moles of the available Cu atoms determined from the effective Cu surface area.

For CZ-post, the Cu and Zn nitrates were precipitated and then added to the carbon precursor solution, and for catalyst CZ-in situ, the Cu and Zn nitrates were co-precipitated directly on the carbon surface. Both of them showed a higher activity. However, C-post and Z-post had very low catalytic activity when only one of the precipitation products was added to another nitrate precursor. According to our previous work [24], the precipitation in the preparation process contains the mixed hydroxides of Cu and Zn that decompose into Cu and Zn oxide clusters, which are further reduced to Cu/ZnO during the carbonization process. Since these Cu/ZnO oxide clusters were formed simultaneously during the formation of the carbon support, they were generally hidden in the carbon support and could not fully access the reaction gas. However, due to the precipitate formed first (CZ-post), this ensured the full contact between Cu and ZnO, which could form the active center of electron transfer and activated the reaction gas, so that the reaction could proceed.

The precipitations of Cu and Zn were directly deposited on the carbon surface or carbon channel structure in CZ-in situ. Hence, more metal and metal oxides were accessible to the reaction gas. Cu and Zn metal oxide nanoparticles formed had higher activity when compared with CZ-post. In other words, for CZ-in situ, not only were the nanoparticles of CuO and ZnO in close proximity, but these metal oxide clusters could also make direct contact with the reaction gas. This was why the activity of CZ-in situ was the highest among

the four catalysts. In addition, the dispersed Cu/ZnO materials were rich in (oxidizable) defects in the ZnO surface, which was expected to be favorable for catalysis [36]. There was a good correlation between the activity of copper/zinc catalysts and copper metal surface area, so high activity in these catalysts is achieved by the preparation of a high dispersion of copper [37,38]. The homogeneous Cu-dispersion usually leads to an equally accessible Cu surface and methanol activities, but there were exceptions. Compared to C-post, Z-post had three times the Cu surface area, but these two catalysts showed similar activity per gram of catalyst. CZ-in situ had a slightly higher Cu surface area than CZ-post, but the catalytic activity was doubled. These two catalysts were much more active than C-post and Z-post. CZ-post and CZ-in situ had more Cu-ZnO interfaces compared to C-post and Z-post. Therefore, we could conclude that other than high Cu surface area, the Cu-ZnO interface was significant to the catalytic activity. A maximized Cu-ZnO interface is crucial for methanol activities.

4. Conclusions

In summary, we demonstrated the synthesis of methanol catalysts with different precursors, i.e., Cu or/and Zn precipitated precursors. The addition of Cu Zn precipitated precursor and co-precipitation on an MC support led to the formation of Cu or CuO/ZnO clusters providing a synergistic effect site. This result was conductive to evenly distributed metal oxide in the catalyst system and showed some catalytic activity. In CZ-in situ, not only were the nanoparticles of CuO and ZnO in close proximity, but these metal oxide clusters could also make direct contact with the reaction gas. It was active for methanol formation with a rate of 0.8 $mmol \cdot g^{-1} \cdot h^{-1}$ and Cu surface area of 3.3 $m^2 \cdot g^{-1}$. Its TOF value (2.8×10^{-3} S^{-1}) was highest but the number of active centers needs to be improved. All results indicate that a better contact between the Cu/CuO and ZnO particles was the active center of the methanol formation. However, the number of active centers needs to be increased.

Author Contributions: Conceptualization; Y.L. and H.D.; methodology; H.D. and G.L.; software, C.W.; formal analysis, Y.F.; data curation, H.D. and Y.F.; writing—original draft preparation, G.L. and Y.L.; writing—review and editing; Y.L. and H.D. All authors have read and agreed to the published version of the manuscript.

Funding: This research was funded by the National Natural Science Foundation of China (project No. 52074051, 51704048), the Natural Science Foundation of Chongqing (No. cstc2020jcyj-msxmX0794) and the fundamental funds for the Central Universities (No. 2020CDJ-LHSs-010).

Institutional Review Board Statement: Not applicable.

Informed Consent Statement: Not applicable.

Acknowledgments: The authors would like to thank Analytical and Testing Center of Chongqing University for N_2 Physisorption, XRD, TG-DTG, SEM, TEM analysis.

Conflicts of Interest: This manuscript is fully original and has not been published before. It is not under our consideration for publication anywhere else. The submission has been approved by all co-authors and the responsible authorities.

References

1. Arán-Ais, R.M.; Dunfeng, G.; Cuenya, R.B. Structure- and Electrolyte-Sensitivity in CO_2 Electroreduction. *Acc. Chem. Res.* **2018**, *51*, 2906–2917. [CrossRef]
2. Schneider, S.H. The Greenhouse Effect: Science and Policy. *Science* **1989**, *243*, 771–781. [CrossRef]
3. Lin, S.; Diercks, C.S.; Zhang, Y.B.; Kornienko, N.; Nickolos, E.M.; Zhao, Y.; Paris, A.R.; Kim, D.; Yang, P.; Yaghi, O.M.; et al. Covalent organic frameworks comprising cobalt porphyrins for catalytic CO_2 reduction in water. *Science* **2015**, *349*, 1208–1213. [CrossRef] [PubMed]
4. O'Neill, S. Global CO_2 Emissions Level Off in 2019, with a Drop Predicted in 2020. *Engineering* **2020**, *6*, 958–959. [CrossRef] [PubMed]
5. Gao, S.; Lin, Y.; Jiao, X.; Sun, Y.; Luo, Q.; Zhang, W.; Li, D.; Yang, J.; Xie, Y. Partially oxidized atomic cobalt layers for carbon dioxide electroreduction to liquid fuel. *Nat. Cell Biol.* **2016**, *529*, 68–71. [CrossRef] [PubMed]

6. Zhang, W.; Hu, Y.; Ma, L.; Zhu, G.; Wang, Y.; Xue, X.; Chen, R.; Yang, S.; Jin, Z. Progress and Perspective of Electrocatalytic CO_2 Reduction for Renewable Carbonaceous Fuels and Chemicals. *Adv. Sci.* **2018**, *5*, 1700275. [CrossRef] [PubMed]
7. Wang, Y.; Gao, W.; Li, K.; Zheng, Y.; Xie, Z.; Na, W.; Jingguang, G.C.; Wang, H. Strong Evidence of the Role of H_2O in Affecting Methanol Selectivity from CO_2 Hydrogenation over Cu-ZnO-ZrO_2. *Chem* **2019**, *6*, 419–430. [CrossRef]
8. Din, I.U.; Shaharun, M.S.; Alotaibi, M.A.; Alharthi, A.I.; Naeem, A. Recent developments on heterogeneous catalytic CO_2 reduction to methanol. *J. CO_2 Util.* **2019**, *34*, 20–33. [CrossRef]
9. Wu, J. Controllable Preparation of Photo-/Electro-Catalytic Materials and Their Catalytic Performance for Carbon Dioxide Reduction. Ph.D. Thesis, University of Science and Technology of China, Hefei, China, 2020.
10. Kattel, S.; Ramírez, P.J.; Chen, J.G.; Rodriguez, J.A.; Liu, P. Active sites for CO_2 hydrogenation to methanol on Cu/ZnO catalysts. *Science* **2017**, *355*, 1296–1299. [CrossRef] [PubMed]
11. Li, C.; Yuan, X.; Fujimoto, K. Development of highly stable catalyst for methanol synthesis from carbon dioxide. *Appl. Catal. A Gen.* **2014**, *469*, 306–311. [CrossRef]
12. Ren, S.; Fan, X.; Shang, Z.; Shoemaker, W.R.; Ma, L.; Wu, T.; Li, S.; Klinghoffer, N.B.; Yu, M.; Liang, X. Enhanced catalytic performance of Zr modified CuO/ZnO/Al_2O_3 catalyst for methanol and DME synthesis via CO_2 hydrogenation. *J. CO_2 Util.* **2020**, *36*, 82–95. [CrossRef]
13. Ren, S.; Shoemaker, W.R.; Wang, X.; Shang, Z.; Klinghoffer, N.; Li, S.; Yu, M.; He, X.; White, T.A.; Ling, X. Highly active and selective Cu-ZnO based catalyst for methanol and dimethyl ether synthesis via CO_2 hydrogenation). *Fuel* **2019**, *239*, 1125–1133. [CrossRef]
14. Nitta, Y.; Fujimatsu, T.; Okamoto, Y.; Imanaka, T. Effect of starting salt on catalytic behaviour of Cu-ZrO_2 catalysts in methanol synthesis from carbon dioxide. *Catal. Lett.* **1993**, *17*, 157–165. [CrossRef]
15. An, H.; Zhang, L.; Zhao, X.; Wang, Y. Effect of preparation conditions on the catalytic performance of Cu–Fe/ZrO2 for the synthesis of DPU from aniline and CO_2. *Chem. Eng. J.* **2014**, *255*, 266–273. [CrossRef]
16. Costantino, U.; Marmottini, F.; Sisani, M.; Montanari, T.; Ramis, G.; Busca, G.; Turco, M.; Bagnasco, G. Cu–Zn–Al hydrotalcites as precursors of catalysts for the production of hydrogen from methanol. *Solid State Ion.* **2005**, *176*, 2917–2922. [CrossRef]
17. Li, J.-L.; Inui, T. Characterization of precursors of methanol synthesis catalysts, copper/zinc/aluminum oxides, precipitated at different pHs and temperatures. *Appl. Catal. A Gen.* **1996**, *137*, 105–117. [CrossRef]
18. Himelfarb, P.; Simmons, G.; Klier, K.; Herman, R. Precursors of the copper-zinc oxide methanol synthesis catalysts. *J. Catal.* **1985**, *93*, 442–450. [CrossRef]
19. Pollard, A.M.; Spencer, S.M.; Thomas, R.G.; Williams, P.A.; HolT, J.; Jennings, J.R. Georgeite and azurite as precursors in the preparation of co-precipitated copper/zinc oxide catalysts. *Appl. Catal. A Gen* **1992**, *85*, 1–11. [CrossRef]
20. Spencer, M. Precursors of copper/zinc oxide catalysts. *Catal. Lett.* **2000**, *66*, 255–257. [CrossRef]
21. Shi, L.; Yang, G.; Tao, K.; Yoneyama, Y.; Tan, Y.; Tsubaki, N. An Introduction of CO2Conversion by Dry Reforming with Methane and New Route of Low-Temperature Methanol Synthesis. *Acc. Chem. Res.* **2013**, *46*, 1838–1847. [CrossRef]
22. Van De Berg, M.W.E.; Polarz, S.; Tkachenko, O.P.; Kähler, K.; Muhler, M.; Grünert, W. Dynamical Changes in the Cu–ZnO_x Interaction Observed in a Model Methanol Synthesis Catalyst. *Catal. Lett.* **2009**, *128*, 49–56. [CrossRef]
23. Van De Berg, M.W.E.; Polarz, S.; Tkachenko, O.P.; Klementiev, K.V.; Bandyopadhyay, M.; Khodeir, L.; Gies, H.; Muhler, M.; Grunert, W. Cu/ZnO aggregates in siliceous mesoporous matrices: Development of a new model methanol synthesis catalyst. *J. Catal.* **2006**, *241*, 446–455. [CrossRef]
24. Duan, H.; Yang, Y.; Singh, R.; Chiang, K.; Wang, S.; Xiao, P.; Patel, J.; Danaci, D.; Burke, N.; Zhai, Y.; et al. Mesoporous Carbon-supported Cu/ZnO for Methanol Synthesis from Carbon Dioxide. *Aust. J. Chem.* **2014**, *67*, 907–914. [CrossRef]
25. Duan, H.; Yang, Y.; Patel, J.; Dumbre, D.; Bhargava, S.K.; Burke, N.; Zhai, Y.; Webley, P.A. A facile method to synthesis a mesoporous carbon supported methanol catalyst containing well dispersed Cu/ZnO. *Mater. Res. Bull.* **2014**, *60*, 232–237. [CrossRef]
26. Ouyang, C.; Wei, H.; Li, Q.; Li, Y.; Duan, H.; Liu, J. Synthesis and Characterization of Catalysts Cu-ZnO Supported on Mesoporous Carbon FDU-15. *J. Chin. Chem. Soc.* **2018**, *65*, 793–800. [CrossRef]
27. Meng, Y.; Gu, D.; Zhang, F.; Shi, Y.; Yang, H.; Li, Z.; Yu, C.; Tu, B.; Zhao, D. Ordered mesoporous polymers and homologous carbon frameworks: Amphiphilic surfactant templating and direct transformation. *Angew. Chem. Int. Ed.* **2005**, *44*, 7053–7059. [CrossRef]
28. Leofanti, G.; Padovan, M.; Tozzola, G.; Venturelli, B. Surface area and pore texture of catalysts. *Catal. Today* **1998**, *41*, 207–219. [CrossRef]
29. Zhang, L.; Lin, J.; Chen, Y. Studies of surface NiO species in NiO/SiO2 catalysts using temperature-programmed reduction and X-ray diffraction. *J. Chem. Soc. Faraday Trans.* **1992**, *88*, 2075–2078. [CrossRef]
30. Behrens, M.; Girgsdies, F.; Trunschke, A.; Schlogl, R. Minerals as Model Compounds for Cu/ZnO Catalyst Precursors: Structural and Thermal Properties and IR Spectra of Mineral and Synthetic (Zincian) Malachite, Rosasite and Aurichalcite and a Catalyst Precursor Mixture. *Eur. J. Inorg. Chem.* **2009**, *2009*, 1347–1357. [CrossRef]
31. Małecka, B.; Gajerski, R.; Małecki, A.; Olszewski, P.; Wierzbicka, M. Mass spectral studies on the mechanism of thermal decomposition of $Zn(NO_3)_2{\cdot}nH_2O$. *Thermochim. Acta* **2003**, *404*, 125–132. [CrossRef]
32. Xia, S.; Yuan, Z.; Wang, L.; Chen, P.; Hou, Z. Hydrogenolysis of glycerol on bimetallic Pd-Cu/solid-base catalysts prepared via layered double hydroxides precursors. *Appl. Catal. A Gen.* **2011**, *403*, 173–182. [CrossRef]
33. Yuan, Z.; Wang, L.; Wang, J.; Xia, S.; Chen, P.; Hou, Z.; Zheng, X. Hydrogenolysis of glycerol over homogenously dispersed copper on solid base catalysts. *Appl. Catal. B Environ.* **2011**, *101*, 431–440. [CrossRef]

34. Duan, H.; Yang, Y.; Patel, J.; Burke, N.; Zhai, Y.; Webley, P.A.; Chen, D.; Long, M. The effect of the modification methods on the catalytic performance of activated carbon supported CuO-ZnO catalysts. *Carbon Lett.* **2018**, *25*, 33–42.
35. Scholten, J.J.F.; Konvalinka, J.A. Reaction of nitrous oxide with copper surfaces. Application to the determination of free-copper surface areas. *Trans. Faraday Soc.* **1969**, *65*, 2465–2473. [CrossRef]
36. Zwiener, L.; Girgsdies, F.; Brennecke, D.; Teschner, D.; Machoke, A.G.; Schlögl, R.; Frei, E. Evolution of zincian malachite synthesis by low temperature co-precipitation and its catalytic impact on the methanol synthesis. *Appl. Catal. B Environ.* **2019**, *249*, 218–226. [CrossRef]
37. Ding, W.; Liu, Y.; Wang, F.; Zhou, S.; Chen, A.; Yang, Y.; Fang, W. Promoting effect of a Cu–Zn binary precursor on a ternary Cu–Zn–Al catalyst for methanol synthesis from synthesis gas. *RSC Adv.* **2014**, *4*, 30677–30682. [CrossRef]
38. Kühl, S.; Friedrich, M.; Armbrüster, M.; Behrens, M. Cu, Zn, Al layered double hydroxides as precursors for copper catalysts in methanol steam reforming–pH-controlled synthesis by microemulsion technique. *J. Mater. Chem.* **2012**, *22*, 9632–9638. [CrossRef]